Ion cyclotron resonance heating-induced density modification near antennas

2013 Plasma Phys. Control. Fusion 55 025002

(http://iopscience.iop.org/0741-3335/55/2/025002)

IOP Publishing Plasma Physics and Controlled Fusion

Plasma Phys. Control. Fusion **55** (2013) 025002 (12pp) doi:10.1088/0741-3335/55/2/025002

Ion cyclotron resonance heating-induced density modification near antennas

Dirk Van Eester, Kristel Crombé and Volodymyr Kyrytsya

Laboratorium voor Plasmafysica-Laboratoire de Physique des Plasmas, Association 'EURATOM-Belgian State', Trilateral Euregio Cluster, Renaissancelaan 30 Avenue de la Renaissance, B-1000, Brussels, Belgium

Received 12 October 2012, in final form 20 November 2012
Published 21 December 2012
Online at stacks.iop.org/PPCF/55/025002

Abstract

By adopting the usual cold plasma dielectric tensor, it is demonstrated that a rapidly oscillating electric field gives rise to slow time scale drifts, which cause density modifications near antennas. In the presence of a strong magnetic field, the poloidal gradients of the field are at the origin of radial displacements of the plasma while radial field gradients have the potential to trigger density inhomogeneity along the antenna. The radio frequency-induced plasma drifts are more prominent at higher power and for more evanescent modes. It is discussed that the usual cold plasma dielectric tensor is derived neglecting nonlinear effects and zero-order drifts, and therefore does not uniformly allow the capture of the wave–particle interaction near the antenna self-consistently, necessitating a more detailed description to capture both wave and particle effects on the one hand, and global wave propagation and local sheath effects, on the other. A strategy is proposed to complement the model with other needed ingredients enabling one to capture the dynamics on the fast and slow time scales.

(Some figures may appear in colour only in the online journal)

1. Introduction

Designing ion cyclotron resonance heating (ICRH) or radio frequency (RF) antennas for application in magnetic confinement fusion machines is commonly carried out by realistically capturing the geometry of the proposed launcher and its environment, but by assuming that the plasma density near the antenna is low enough to justify neglecting its presence altogether, or by substituting the plasma by a simple dielectric (see, e.g., [1, 2]). As wave coupling critically depends on the density profile the antenna faces [3–5], such near-field computations are commonly interfaced with core wave equation solvers to account for the impact the plasma has on the emitted waves; one of the more powerful approaches is due to the Politecnico Group of Torino (see, e.g., [6]) in which a one-dimensional (1D) hot plasma-wave equation solver FELICE is interfaced with the TOPICA antenna code via the surface impedance matrix.

Hence, at best, the plasma density is assumed *known* and prescribed when performing antenna computations. Experimentally it has, however, been observed on many machines that the density is *modified* by the presence of the waves (see, e.g., [3, 7]). The higher the wave power, the more will be the change in density in the region in front of the antenna. Also, heating scenarios characterized by low single pass absorption tend to affect the density more than scenarios with good heating efficiency. Both effects are thought to be due to RF sheaths (see, e.g., [7–13]) but details of the interaction mechanism are still under further study. In view of the fact that the coupling of wave power is a very sensitive function of density, a better understanding of the plasma dynamics would allow one to understand (and if possible reverse) the adverse impact high-power wave excitation has on the plasma in front of the launcher. For some of the aspects of the near-field physics, expressions have been derived that only partly account for the wave dynamics and typically rely on a number of assumptions that are not uniformly justified (see, e.g., [9, 13]), while a fully self-consistent description would require solving the system of coupled equations containing at least Maxwell's equations and the relevant equations of motion and continuity for each of the plasma constituents. As averaging over the fast time scale of the driven oscillation at frequency ω adds nonzero (quasilinear) terms that need to be accounted for when solving the slow time scale phenomena, such modeling is quite involved and has so far never been attempted for antenna modeling in the ICRH domain when including effects such as RF-induced sheaths. This paper adopts an intermediate philosophy and aims at qualitatively assessing the effect of RF power on density in the neighborhood of an antenna. It starts from the assumption that the usual

cold plasma description due to Stix (see, e.g., [14, 15]) allows capturing all important fast time scale dynamics to compute the electric field pattern, and then introduces the obtained results into an analytical expression for wave-induced zero-order drifts. This drift velocity prediction is then introduced into the continuity equation to give a first estimate of the wave-induced density modification.

This paper's modest aim is to illustrate the following two points:

(i) Whereas RF sheath effects are commonly attributed to the electric field component *parallel* to the magnetic field, it is argued here that both parallel and perpendicular wave components give rise to drifts that can cause density modifications and thus need to be retained in the description. Effects on the Debye length require a dedicated treatment and are *not* included in the present model; although they will be discussed in more detail elsewhere [16], the very specific dynamics in the region where the charge neutrality is strongly violated due to the proximity of a metallic object will very briefly be touched upon in the section on the comparison with other relevant drifts of the RF-induced drift velocity derived next. In the presence of a strong magnetic field the poloidal gradients of the field are at the origin of radial displacement of the plasma while radial field gradients have the potential to trigger density inhomogeneity along the antenna.

(ii) The results obtained reveal that more rigorous modeling is required to capture the wave–particle interaction near the antenna fully self-consistently. However, the obtained drift velocities are very small with respect to the species' thermal velocities so that—with the exception of sheath physics aspects—the obtained results should be indicative of the onset of density modification.

This paper is structured as follows: first, a generalization of the ponderomotive force in the presence of a strong magnetic field is derived. Then, the adopted cold plasma-wave model is discussed. After that, a method is proposed to qualitatively describe the RF-induced density modification. After that, an example is presented, after which the road ahead is sketched. Conclusions are drawn in the final section.

2. Ponderomotive force in the presence of a strong magnetic field

The ponderomotive acceleration a population of particles undergoes as a net result of an inhomogeneous electric field $\vec{E}$ driven at a frequency ω is given by

$$\vec{a}_{\rm Pon} = -\nabla |\frac{q}{2m\omega}\vec{E}|^2$$

(see, e.g. the derivation in [15]). As this expression was derived in the absence of a magnetic field, it cannot be directly applied to the case of charged particles in a magnetic confinement fusion machine, where the particle orbits are dominantly imposed by the confining field. Adopting the same philosophy, this classical result can, however, be readily generalized. The relevant fluid-type equation of motion for each type of particles is

$$Nm\frac{\rm d}{{\rm d}t}\vec{v} = -\nabla NkT + qN\vec{E}{\rm e}^{-{\rm i}\omega t} + qN\vec{v}\times\vec{B}_o$$

(N is the density, m is the mass, T is the temperature, q is the charge and $\vec{v}$ is the velocity of the flow of one of the types of particles in the plasma), which—for constant temperature—can more compactly be rewritten as

$$\frac{\rm d}{{\rm d}t}\vec{v} = -v_t^2\frac{\nabla N}{N} + \vec{\epsilon}{\rm e}^{-{\rm i}\omega t} + \Omega\vec{v}\times\vec{e}_\parallel$$

with $v_t^2 = kT/m$, $\vec{\epsilon} = q\vec{E}/m$, $\Omega = qB_o/m$ and $\vec{e}_\parallel = \vec{B}_o/B_o$; note that—in line with what is carried out in deriving the usual cold plasma dielectric tensor—the *driven* magnetic field is neglected since it is a small correction to the terms retained. We will assume that the static magnetic field $\vec{B}_o$ is straight and homogeneous. Anticipating that the motion can be split into a fast dynamics part, which responds on the time scales imposed both by the generator and the strong confining magnetic field, and a slow dynamics part, which accounts for the remaining net drifts when averaging over all fast time scales, we split both velocity $\vec{v} = \vec{v}_o + \vec{v}_1$ and position $\vec{x} = \vec{x}_o + \vec{x}_1$ into a zero-order and a perturbed part. The electric field is inhomogeneous in general. Assuming the perturbation is small and thus following the same philosophy as for the derivation of the ponderomotive force, $\vec{\epsilon}$ can be approximated by the truncated Taylor series expansion

$$\vec{\epsilon}(\vec{x}) \approx \vec{\epsilon}(\vec{x}_o) + (\vec{x} - \vec{x}_0).\nabla\vec{\epsilon}(\vec{x}_o),$$

so that the fast dynamics is governed by the equation

$$\frac{\rm d}{{\rm d}t}\vec{v}_1 = +\vec{\epsilon}(\vec{x}_o){\rm e}^{-{\rm i}\omega t} + \Omega\vec{v}_1\times\vec{e}_\parallel,$$

for which it has been assumed that the fast scale density variations are either absent or can be neglected ($N \approx N_o$), while the slow dynamics are captured by

$$\frac{\rm d}{{\rm d}t}\vec{v}_o = -v_t^2\frac{\nabla N_o}{N_o} + \frac{1}{2}{\rm Re}[\langle(\vec{x}^* - \vec{x}_0^*).\nabla\vec{\epsilon}(\vec{x}_o){\rm e}^{-{\rm i}\omega t}\rangle] + \Omega\vec{v}_o\times\vec{e}_\parallel$$

with $\langle\ldots\rangle$ representing the averaging over all fast oscillations and '*' denoting the complex conjugate. Solving the equation of motion for the fast dynamics yields

$$x_{\perp 1} = x_{\perp 1,0} + \frac{1}{2}\left[\frac{v_{+0}}{-{\rm i}\Omega}{\rm e}^{-{\rm i}\Omega t} + \frac{v_{-0}}{{\rm i}\Omega}e^{{\rm i}\Omega t}\right] - \frac{\omega\epsilon_{\perp 1} + {\rm i}\Omega\epsilon_{\perp 2}}{\omega(\omega^2 - \Omega^2)}{\rm e}^{-{\rm i}\omega t}$$

$$x_{\perp 2} = x_{\perp 2,0} + \frac{1}{2i}\left[\frac{v_{+0}}{-{\rm i}\Omega}{\rm e}^{-{\rm i}\Omega t} - \frac{v_{-0}}{{\rm i}\Omega}e^{{\rm i}\Omega t}\right] - \frac{\omega\epsilon_{\perp 2} - {\rm i}\Omega\epsilon_{\perp 1}}{\omega(\omega^2 - \Omega^2)}{\rm e}^{-{\rm i}\omega t}$$

$$x_\parallel = x_{//0} + v_{//0}t - \frac{\epsilon_\parallel}{\omega^2}{\rm e}^{-{\rm i}\omega t}.$$

The motion perpendicular to the static magnetic field contains a constant contribution, an oscillatory contribution that responds

to the cyclotron motion imposed by the static magnetic field and a driven oscillatory contribution that corresponds to the movement caused by the electric field. Since the magnetic field does not exert any influence parallel to its field lines, the parallel motion is only constituted of the guiding center drift along the magnetic field line and resulting from the initial velocity $v_{//0}$, and the driven response to the electric field.

In tokamaks, the magnetic field is of the order of a few tesla, while the electric field excited by RF antennas is commonly of the order of a few 10^4 V m^{-1}. Taking the thermal velocity as a measure for the typical velocities reached, the velocity is of order 10^4 ms^{-1} for typical edge temperatures of a few eV. Hence, the cyclotron gyration term and the electric field term are of equal importance in the edge: $|E/[vB_o]| \approx 1$. This has profound consequences since it undermines the concept of magnetic surfaces close to the RF antennas for sufficiently powerful RF waves. In the hot plasma core, where the electric field is propagative rather than evanescent, the more customary $|E/[vB_o]| \ll 1$ holds.

With the obtained expressions, the ponderomotive term in the presence of a strong magnetic field can now be evaluated. Retaining only the net nonoscillatory terms one finds

$$\vec{a}_{\rm Pond} = -\frac{1}{2}{\rm Re}\Big[+ \frac{1}{\omega(\omega^2-\Omega^2)}\left(\left[\omega\epsilon^*_{\perp 1} - {\rm i}\Omega\epsilon^*_{\perp 2}\right]\frac{\partial}{\partial x_{\perp 1}}\vec{\epsilon}\right.$$
$$\left. + \left[\omega\epsilon^*_{\perp 2} + {\rm i}\Omega\epsilon^*_{\perp 1}\right]\frac{\partial}{\partial x_{\perp 2}}\vec{\epsilon}\right) + \frac{1}{\omega^2}\epsilon^*_{\parallel}\frac{\partial}{\partial x_{\parallel}}\vec{\epsilon} - \frac{iv^*_{//0}}{\omega}\frac{\partial}{\partial x_{\parallel}}\vec{\epsilon}\Big], \quad (1)$$

in which the functions appearing in the cold plasma dielectric tensor elements (see, e.g., [14]) can be recognized and in which the last term appears only in the case where there is a finite zero-order parallel drift velocity $v_{//0}$ in the absence of the RF field. Note that the ponderomotive acceleration goes to infinity at cyclotron layers. Whereas this paper adopts a cold plasma representation suitable for the antenna region, Fukuyama *et al* [17] studied wave induced flow accounting for finite temperature effects. Their paper also provides the MHD limit of the obtained warm plasma expression for slab geometry, weak inhomogeneity and in the electrostatic limit without zero order drifts. Using the notation adopted in this paper, that expression reads

$$\vec{a}_{\rm Pond} = -\frac{1}{2}{\rm Re}\Big[\nabla\Big(\frac{|\epsilon_\perp|^2}{\omega^2-\Omega^2} + \frac{|\epsilon_\parallel|^2}{\omega^2}\Big)\Big].$$

It elegantly highlights the main change to the usual ponderomotive acceleration added by the static magnetic field. In the same limit, the earlier presented expression, equation (1) for the ponderomotive force reduces to the result due to Fukuyama *et al*. Because it allows for electromagnetic as well as electrostatic fields just like the standard ponderomotive acceleration, equation (1) and not its simpler limit will be used for the application discussed in section 5.

Putting the obtained expression for the ponderomotive acceleration into the equation of motion for the slow dynamics, the latter can also be solved in a similar way as the equation of the fast dynamics. For typical parameters in the plasma edge, the two accelerations in $\tilde{\vec{a}} = -v_t^2[\nabla N_o]/N_o + \vec{a}_{\rm Pond}$ are of similar magnitude, while the Lorentz force of the confining field is significantly larger. By first dropping the acceleration $\tilde{\vec{a}}$ due to the slow dynamics and then solving the full equation by variation of the constants, one obtains $v_{o,\perp 1} = +\tilde{a}_{\perp 2}/\Omega$, $v_{o,\perp 2} = -\tilde{a}_{\perp 1}/\Omega$ which is of the usual form

$$\vec{v}_{{\rm drift},\perp} = \frac{\vec{F}\times\vec{B}_o}{qB_o^2}$$

of drift velocities in the presence of a magnetic field together with another force $\vec{F} = m\vec{a}$. As the magnetic field does not influence the parallel dynamics, this drift velocity is perpendicular to the confining field while the parallel dynamics is identical to the case in the absence of $\vec{B}_o$. Note that for ion species whose fundamental cyclotron layer lies in the antenna region, the ponderomotive force effect is strongly enhanced compared with the case in the absence of a magnetic field. Apart from the antenna near-field application discussed in this paper, the obtained ponderomotive force expression thus allows one to qualitatively describe how a poloidal rotation/flow is set up near the cyclotron resonance. The behavior exactly at the cyclotron resonance would require special attention since $\Omega = \omega$ invalidates the assumption that was made on the distinction between slow and fast particle dynamics because terms proportional to $\exp[{\rm i}(\Omega-\omega)t]$ then are constant rather than rapidly varying, but in the high-frequency domain one need not be separated far from the actual cyclotron resonance for the mentioned beating term to vary much more rapidly than the slow time scale variations.

Compared with the $\vec{B}_o$-less case, the direction of the net motion of the particles has changed. Rather than creating an acceleration that is mainly in the direction of the strongest gradient of the magnitude of the electric field, a drift perpendicular to the $\vec{B}_o$ field and perpendicular to the ponderomotive force is created. When $\vec{B}_o = \vec{0}$, the ponderomotive effect radially chases particles away from the antenna region due to the radial field gradient, whereas $\vec{B}_o \neq \vec{0}$ requires the *poloidal* gradient of the electric field to cause a radial drift, the magnitude of which is decided by the difference between the frequency and the cyclotron frequency. At the top of the antenna, this radial drift is opposite to that at the bottom. The *radial* component of the ponderomotive force together with the toroidal field yields an upward or downward poloidal motion along the antenna. Since the evanescent electric field decays exponentially away from the antenna (in vacuum $k_\perp^2 = k_o^2 - k_\parallel^2 \approx -k_\parallel^2$ so the field decays as $\exp[-k_\parallel|x-x_{\rm ant}|]$ for most $k_\parallel \gg k_o$ in the antenna spectrum), the various effects together give rise to a particle streaming along the antenna, a depopulation at one end of the antenna and a population at the other. Although the density in front of the antenna is poloidally homogeneous at the outset, the RF waves themselves thus set up a poloidal density asymmetry.

3. Wave model

As the edge temperature is low, finite temperature effects are of little significace in the wave model, and the usual cold plasma model (see, e.g., [14, 15]) seems adequate. Although intended to shed light on wave excitation in tokamaks, curvature effects are assumed nonessential here, hence a slab model is used.

The x-coordinate parametrizes the radial direction, the y-coordinate labels the poloidal direction, and z the toroidal direction. The magnetic field is assumed *constant* but generally has a poloidal apart from its toroidal dominant component. The angle between the toroidal direction and the static magnetic field will be labeled α. The antenna poloidal and toroidal spectrum is determined accounting for the periodicity in the poloidal and toroidal directions, i.e. k_y and k_z are considered constant but their values are determined by the poloidal (m) and toroidal (n) mode numbers and the antenna minor ($r_{\rm ant}$) and major ($R_{\rm ant}$) radius: $k_y = k_{y,m} = m/r_{\rm ant}$ and $k_z = k_{z,n} = n/R_{\rm ant}$. The antenna toroidal width and poloidal length then determine the Fourier amplitudes of the antenna current, which is assumed to be confined to a magnetic surface, i.e., $\vec{J}_{\rm ant}(\vec{x}) = \vec{J}\delta(x - x_{\rm ant})$, but having constant poloidal (J_y) and toroidal (J_z) components on the antenna surface:

$$\vec{J}_{\rm ant} = \left(\frac{1}{\pi}\right)^2 \sum_m \sum_n \frac{\sin(k_{y,m} w_y/2)}{m} \frac{\sin(k_{z,n} w_z/2)}{n} \times [J_y \vec{e}_y + J_z \vec{e}_z]. \tag{2}$$

In terms of the discrete set of $(k_y, k_z) = (k_{y,m}, k_{z,n})$ values and eliminating the magnetic field, the wave equation can be written as

$$\left[\begin{pmatrix} k_y^2 + k_z^2 & 0 & 0 \\ 0 & k_z^2 & -k_y k_z \\ 0 & -k_y k_z & k_y^2 \end{pmatrix} + \begin{pmatrix} 0 & {\rm i}k_y & {\rm i}k_z \\ {\rm i}k_y & 0 & 0 \\ {\rm i}k_z & 0 & 0 \end{pmatrix} \frac{\rm d}{{\rm d}x} + \begin{pmatrix} 0 & 0 & 0 \\ 0 & -1 & 0 \\ 0 & 0 & -1 \end{pmatrix} \frac{{\rm d}^2}{{\rm d}x^2} \right] \begin{pmatrix} E_x \\ E_y \\ E_z \end{pmatrix} = {\rm i}\omega\mu_0 \vec{J}_{\rm ant} + k_0^2 \overline{\overline{R}}.\overline{\overline{K}}_{\rm NR}.\overline{\overline{R}}^{-1} \tag{3}$$

in which $\overline{\overline{K}}_{\rm NR}$ is the usual nonrotated cold plasma dielectric tensor with respect to the $\vec{B}_o$-based directions $(\vec{e}_{\perp,1}, \vec{e}_{\perp,2}, \vec{e}_\parallel) = (\vec{e}_x, \cos\alpha\vec{e}_y - \sin\alpha\vec{e}_z, \sin\alpha\vec{e}_y + \cos\alpha\vec{e}_z)$ and $\overline{\overline{R}}$ is the rotation matrix for transforming vectors from the $(\vec{e}_{\perp,1}, \vec{e}_{\perp,2}, \vec{e}_\parallel)$-based to the $(\vec{e}_x, \vec{e}_y, \vec{e}_z)$-based frame. As E_x for each (k_y, k_z) is a linear combination of the other two wave components and their first derivatives, it can be eliminated when solving the system.

Four boundary conditions are required to uniquely define a solution of this fourth-order differential equation. The boundary conditions at the metallic wall are $E_y = E_z = 0$, and two radiating conditions are imposed at the interface of the region of interest with the deeper plasma core. To interface the solutions at either side of the antenna four conditions are needed: (i) two jump conditions for the derivatives $[{\rm d}E_y/{\rm d}x]_{x_{\rm ant}^-}^{x_{\rm ant}^+} = +{\rm i}\omega\mu_o J_y$, $[{\rm d}E_z/{\rm d}x]_{x_{\rm ant}^-}^{x_{\rm ant}^+} = -{\rm i}\omega\mu_o J_z$ describe the power fed into the system at the antenna location $x_{\rm ant}$, and (ii) the requirement that E_y and E_z themselves are continuous there.

Assuming the wave power is efficiently absorbed inside the plasma, antenna modeling is commonly done imposing radiating boundary conditions, i.e. assuming that neither of the waves the plasma admits can carry energy *into* the antenna region from the plasma side. Assuming the waves are decoupled (the WKB condition satisfied) at the plasma interface, the usual cold plasma dispersion equation—found by substituting ${\rm d}/{\rm d}x \to {\rm i}k_x$ in the above wave equation and omitting the antenna term—can be solved and the four possible kinds of waves (two of the fast wave and two of the slow wave type) are identified. Solving the polarization equation for each of the wave types ζ with dispersion root $k_x = k_\zeta$ yields the eigenvectors $(1, {\rm i}k_\zeta, E_z/E_y|_\zeta, {\rm i}k_\zeta E_z/E_y|_\zeta)$. The independent variables and the eigenvectors are related by the matrix $\overline{\overline{T}}$:

$$\begin{pmatrix} E_y \\ {\rm d}E_y/{\rm d}x \\ E_z \\ {\rm d}E_z/{\rm d}x \end{pmatrix} = \overline{\overline{T}}. \begin{pmatrix} s_{{\rm FW},\rightarrow} \\ s_{{\rm FW},\leftarrow} \\ s_{{\rm SW},\rightarrow} \\ s_{{\rm SW},\leftarrow} \end{pmatrix} = \begin{pmatrix} 1 & 1 & \dots \\ {\rm i}k_{{\rm FW},\rightarrow} & {\rm i}k_{{\rm FW},\leftarrow} & \dots \\ E_z/E_y|_{{\rm FW},\rightarrow} & E_z/E_y|_{{\rm FW},\leftarrow} & \dots \\ ({\rm i}k_{{\rm FW},\rightarrow})(E_z/E_y|_{{\rm FW},\rightarrow}) & ({\rm i}k_{{\rm FW},\leftarrow})(E_z/E_y|_{{\rm FW},\leftarrow}) & \dots \end{pmatrix} . \begin{pmatrix} s_{{\rm FW},\rightarrow} \\ s_{{\rm FW},\leftarrow} \\ s_{{\rm SW},\rightarrow} \\ s_{{\rm SW},\leftarrow} \end{pmatrix} \tag{4}$$

and hence preventing the fast or slow wave from carring energy into the interval requires imposing the conditions $s_{{\rm FW},\rightarrow} = 0$ and $s_{{\rm SW},\rightarrow} = 0$. The described set of conditions now uniquely defines the solution in the region of interest. Using $\vec{s} = \overline{\overline{T}}^{-1}.\vec{Y}$—where $\vec{Y}$ is the four-vector of independent variables $(E_y, {\rm d}E_y/{\rm d}x, E_z, {\rm d}E_z/{\rm d}x)$—other choices of two boundary conditions at the plasma side can be imposed if so desired.

4. Wave-induced density modification

Once the solution of the equation of motion is known, the density modification for each type of species can be evaluated using the continuity equation,

$$\frac{\partial}{\partial t} N_o + \nabla.[\vec{v}_{\rm drift} N_o] = 0.$$

Since the density in the scrape-off layer of tokamak plasmas and close to the antennas is expected to vary significantly over short distances, it is numerically more convenient to solve the equivalent equation

$$\frac{\partial}{\partial t} \log_{10} N_o = -\vec{v}_{\rm drift}.\nabla \log_{10} N_o - \nabla.\vec{v}_{\rm drift},$$

which can be solved by time stepping starting from an initial profile. As the pressure term $-v_t^2[\nabla N_o]/N_o$ in the drift velocity itself depends on the density and its gradient, directly solving the above equation, assuming that a stationary state can be reached, does not yield physically meaningful results as N_o is yet unknown. Moreover, because already in the absence of RF waves the density decays exponentially just outside the last closed flux surface, directly solving that equation is numerically challenging. Gradually switching on the density modification terms—substituting the nonlinear problem by a series of linear ones iteratively solved using the results obtained in the previous iteration in the next step's nonlinear terms while introducing a switch-on coefficient in front of the nonlinear terms that smoothly varies from 0 at the first iteration to 1 at the last—in the time-dependent solution

proved to be a suitable numerical procedure; 1000 iteration steps together with a leveling-off of the switch-on function guaranteed convergence of the procedure. Whereas solving the nonlinear equations as a series of linear ones allows one to find the stationary state solution quickly, it comes with a price: the time derivatives can no longer be considered as representing the actual temporal evolution of the system. Adopting a finite difference scheme with a suitably small time step would be a—be it time consuming—alternative. Consistent with the earlier introduced angle α between the magnetic field and its toroidal projection, the drift velocity consistent with the pressure gradient term $-v_{\rm th}^2[\nabla N]/N$ is

$$\vec{v}_{\text{no-RF}} = -\frac{v_{\rm th}^2}{N_o\Omega}\left[\cos\alpha\left(\frac{\partial N_o}{\partial y}\vec{e}_x - \frac{\partial N_o}{\partial x}\vec{e}_y\right) + \sin\alpha\frac{\partial N_o}{\partial x}\vec{e}_z\right],$$

the divergence of which is zero. Although the initial density has only a radial dependence, poloidal inhomogeneities emerge at a later stage due to the above drift velocity.

The result obtained by iteratively solving the present equation for a given electric field profile does not yield a fully self-consistent solution but only yields a qualitative description of the first step in this process. A more sophisticated model requires the electric field profile itself to be evolved accordingly and requires solving the wave equation for a 2D density profile, opposite to what was done in this paper where the density is assumed to depend only on x. Moreover, other effects (such as transport, see, e.g., [18]) are likely to contribute to the density evolution. Finally, as zero-order drifts are created by the RF electric field, a wave model relying on the classical cold plasma dielectric tensor—which was derived by assuming that zero-order drifts are absent and by omitting nonlinear terms in the equation of motion—is insufficient to describe the wave dynamics accurately. However, the drift velocities are small with respect to the species' thermal velocities so that—with the exception of sheath physics aspects, which occur on the very short length scale of the Debye length and where the velocity build-up can be significant (aspects ignored in this paper but addressed in an accompanying one [16] because of their highly specific but very localized footprint)—the obtained results should be indicative of the onset of density modification but are believed to be too crude to justify actual time stepping at this stage; see the discussion on the way ahead in the last section.

5. Numerical example

An example loosely inspired on JET parameters is discussed next. Figure 1 shows the real and imaginary parts of the electric field components for an antenna situated at $R = R_o + x_{\rm ant} = 4.05$ m and with a current density with a dominantly poloidal ($J_y = -10^4\,\mathrm{A\,s^{-1}\,m^{-3}}$) but also a toroidal ($J_z = 10^3\,\mathrm{A\,s^{-1}\,m^{-3}}$) current density. The latter choice is based on the realization that although one experimentally tries to launch 'pure' fast or slow waves by orienting the antennas appropriately ($J_y \neq 0$ or $J_z \neq 0$, respectively), full wave antenna computations show that currents on the launchers often acquire a parasitic current density component exciting the nondesired mode when fields around and currents on realistic antenna structures are self-consistently computed; an example of such currents can be found in [19]. Depending on the density (determining whether the slow/fast wave is evanescent or propagative close to the antenna), the impact of the parasitically excited slow/fast wave may be more or less strongly felt away from the antenna. An exponential decay length of $\lambda_N = 0.01$ m was assumed with a reference electron density of $5\times10^{16}\,\mathrm{m^{-3}}$ at $R = 3.8$ m and considering a $(H) - D$ minority scenario with $X[H] = N_{\rm H}/N_e = 5\%$ in a JET-like geometry with major radius of $R_o = 3$ m and minor radius $a_{\rm p} = 0.9$ m. Furthermore, $f = 51$ MHz and $B_o(R_o) = 3.45$ T corresponding to central ion heating at the fundamental H and second harmonic D cyclotron layer in the core of the plasma but taking the appropriate B_o at the antenna level for local consistency; a uniform collision frequency of $\nu = 10$ kHz was adopted and $\alpha = 0.2$ rad. The antenna spectrum was modeled using 51 poloidal modes but only a single toroidal mode ($n = 26$, the dominant mode for dipole heating of the JET A2 antenna [20]) was retained. Due to the exponentially decaying density parameters, the lower hybrid resonance is crossed behind the antenna and the slow wave remains propagative up to the back wall. Its signature can clearly be seen on the radial component of the electric field while the poloidal component does not reveal a trace of it. To ensure that the subtleties of the short-wavelength wave are captured, 350 radial points were used for performing the computation. Whereas antenna modeling is often performed neglecting the plasma effects or considering a purely fast wave excitation, figure 1 shows that both the fast and slow wave play a role at the very low densities deep behind the last closed flux surface characteristic for the antenna region and that the wave–wave interaction dynamics or direct excitation of either wave by antenna current densities that are not purely poloidal or toroidal should be accounted for.

Figure 2 depicts the radial and poloidal components of the wave-induced drift velocity; the antenna is at the extreme right of the picture and poloidally extends from -0.1 m to $+0.1$ m while a poloidal region of twice that size is considered. Very close to the antenna the drift velocity is (poloidally) upward for the ions and downward for the electrons; the poloidal flow is very strong close to the launcher and quickly decreases away from it. This is the drift caused by the radial decay of the electric field strength. Away from the antenna the drift is toward the antenna for ions at the top end of the strap and away from it at the bottom; the electron response is in the opposite direction. Overall, one thus expects the formation of an excess of positive charge at one antenna poloidal end and a deficiency at the other.

Figure 3 shows an example of this density deformation by iterative solving of the continuity equation for a given RF field pattern in the region in front of the antenna. At the left, the density change due to the pressure term is visible. On the right (close to the antenna), the RF wave dynamics is dominant. On top of the population/depopulation at the poloidal ends of the antenna, one observes that the poloidal drifting of the majority ions along the antenna causes an up–down asymmetry of the majority density the antenna faces. The electrons show the opposite tendency.

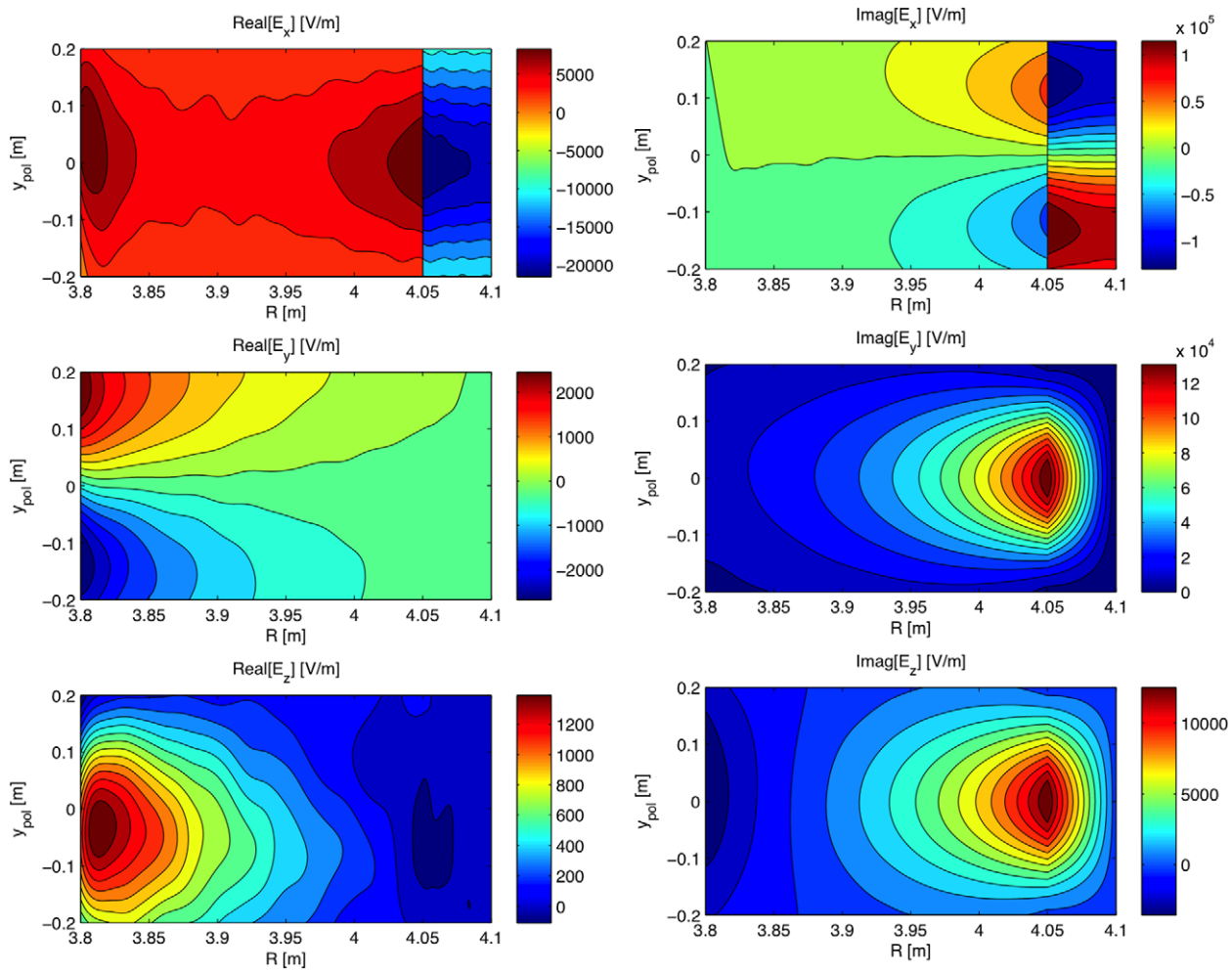

Figure 1. Example of the real and imaginary parts of the three electric field components.

In the first example the current density on the antenna was imposed. From the expressions of the drift velocity one directly concludes that the drift velocity magnitude scales with the square of the electric field and thus with the power if all other quantities remain unchanged. The wave pattern and magnitude evidently depend on other parameters as well, the launched wave spectrum being one of the more important ones. Figures 4 and 5 give an idea of the velocity variation along and perpendicular to the antenna, and how the velocity changes as a function of the toroidal mode number. The core density is $3 \times 10^{19}\,\mathrm{m}^{-3}$ and the density at the last closed flux surface $R = 3.9\,\mathrm{m}$ is $10^{19}\,\mathrm{m}^{-3}$. In the scrape-off layer an exponential decay with characteristic length of 0.02 m is assumed. The other parameters are as before but three toroidal mode numbers 13, 26 and 39 are considered while an antenna width of 0.3 m was taken; the former and the latter are the locations of the dominant and next-to-dominant mode number peaks for the current drive spectrum of the A2 JET antennas while the second value is where the maximum lies for dipole (heating) phasing. The antenna is placed at $R = 3.95\,\mathrm{m}$.

The drift velocities are depicted for 1 MW launched into the machine and the poloidal antenna spectrum is described using 31 poloidal modes. The first observation from figure 4 is that the magnitude of the ion drift velocity is globally larger for lower toroidal mode numbers, underlining the interplay between the density and the toroidal wave spectrum in determining whether the excited (mainly fast) wave is propagative, barely evanescent or deeply evanescent. Recall that—to a large extent and because the finite confining magnetic field causes different dynamics in different directions—the ponderomotive force for each of the particle types is along the main gradient of the relevant electric field component. Compared with the thermal velocity, the RF-induced electron drift is negligible so other dynamics likely need to be included to assess the fate of the electrons. Near the tips of the antenna $|y| = 0.15\,\mathrm{m}$ the ion drift velocity components reach a maximum. The v_x component shows that ions stream toward the antenna at the bottom of the antenna and are chased away from it at the top. Along the antenna (v_y) the particles tend to stream upward. This streaming is more pronounced for smaller n_{tor} and is significantly larger than the radial streaming. On the 2D plots shown before and confirmed by figure 5 it was shown that this component dies away quickly away from the antenna. For the adopted parameters, the effect of the RF waves happens relatively close to the antenna in a region of about 5 cm width. The extent of this region is closely connected to the local density. Also (not visible in front of the antenna for the present parameters) the *propagative* slow

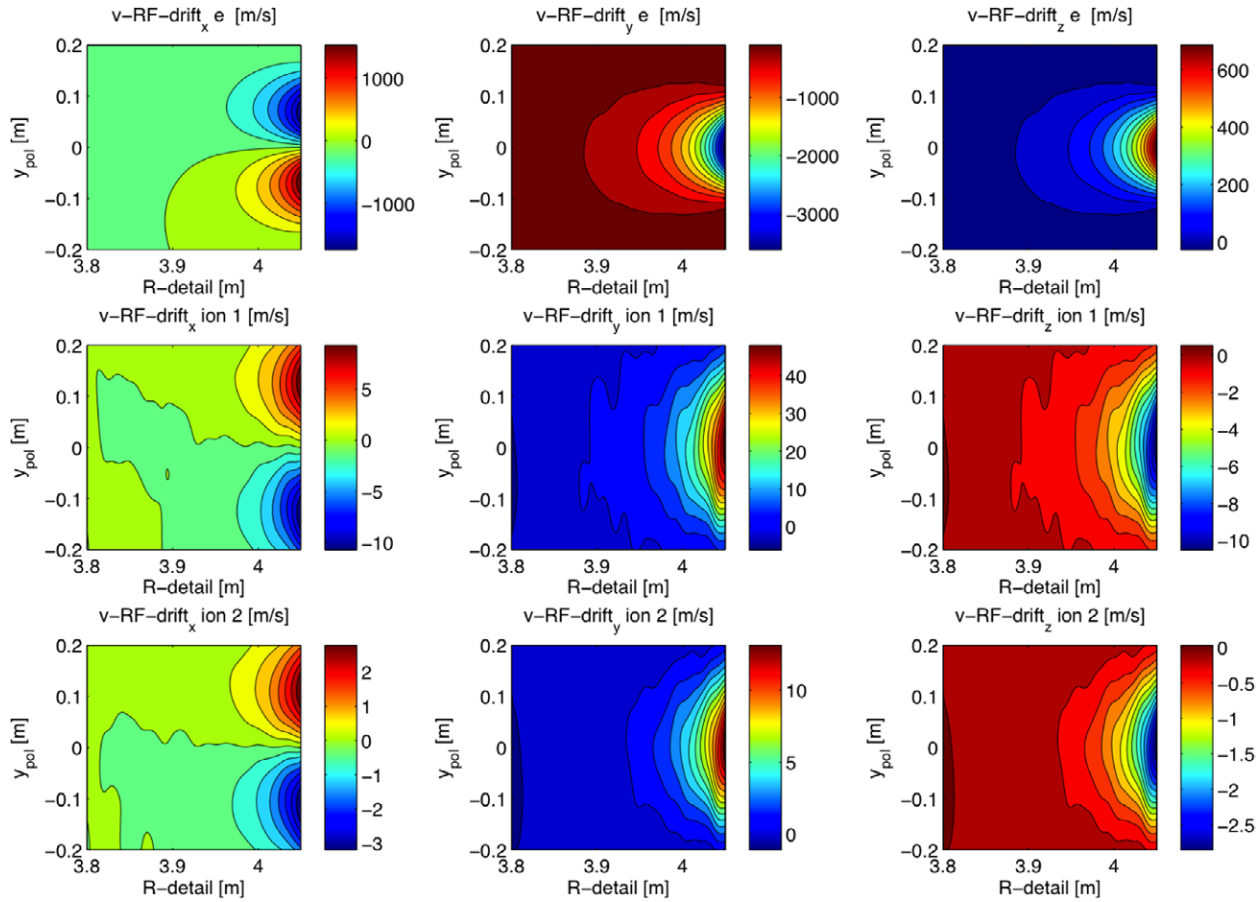

Figure 2. Radial (x, left), poloidal (y, middle) and toroidal (z, right) components of the wave-induced velocity drift for electrons (top), minority H (middle) and majority D (bottom) ions in front of the antenna over double the antenna poloidal length distance.

wave has a more prominent signature when the density falls under the lower hybrid density. The specific effect of the sheath that is formed in the first few Debye lengths just in front of the antenna is *not* addressed here since the density profile that is set up due to the charge separation is not self-consistently accounted for; it is the subject of a separate paper and of a vast research effort (see [16] and references therein).

Not only in the radial and poloidal directions but also in the toroidal one, particles are moved into or out of the antenna environment ($\alpha \neq 0$). Recall that the present simple model does not include an antenna box. The motion is likely to be different when the effect of the antenna box is added to the computation. Nevertheless, the simple computations demonstrate that the RF waves induce flows on the slow time scale that will modify the density and that should be taken into account. The drifts add to the physics on the diffusion time scale. They are tiny compared with the thermal velocity of the particles and hence partly justify the use of the zero-net-drift cold plasma dielectric tensor; in the sheath omitted here more prominent velocities are found.

Consistent with experimental observations, the RF-induced drift is more pronounced for lower $k_\parallel$. However, the difference between the various antenna phasings is underestimated in the present computation: at low $k_\parallel \approx n_{\rm tor}/R$, the single pass absorption for the H minority heating scheme is poor (10–20% as opposed to 100% single pass absorption characteristic for higher $k_\parallel$ [21]). As a consequence, and with the exception of destructive interference at specific densities, the waves are sloshing over the plasma many times before being absorbed, and the edge electric field is significantly larger for such cases. As radiative boundary conditions were adopted in the present computation, it was assumed that no power ever makes it back to the antenna at any $k_\parallel$, an assumption that is clearly violated at low $n_{\rm tor}$. As a consequence, the amplitude of the drift velocity magnitudes is underestimated.

The charge separation that results from the net velocity drifts will cause an electrostatic field to be set up along the antenna and—in conjunction with the confining magnetic field—will cause a radial $\vec{E} \times \vec{B}_o$ drift of both ions and electrons. Neither the RF-induced velocity drift nor the electrostatic field it causes are accounted for in the cold plasma description that was adopted at the outset of this study. Hence, the present results are qualitative and mainly serve to illustrate that the RF-induced drifts are important and should be accounted for. A more rigorous description is proposed in the final section.

6. Towards a self-consistent description

With the exception of the case where the region of interest is close to the cyclotron layer of one of the ion species (yielding much larger perturbations), the drift velocity derived here

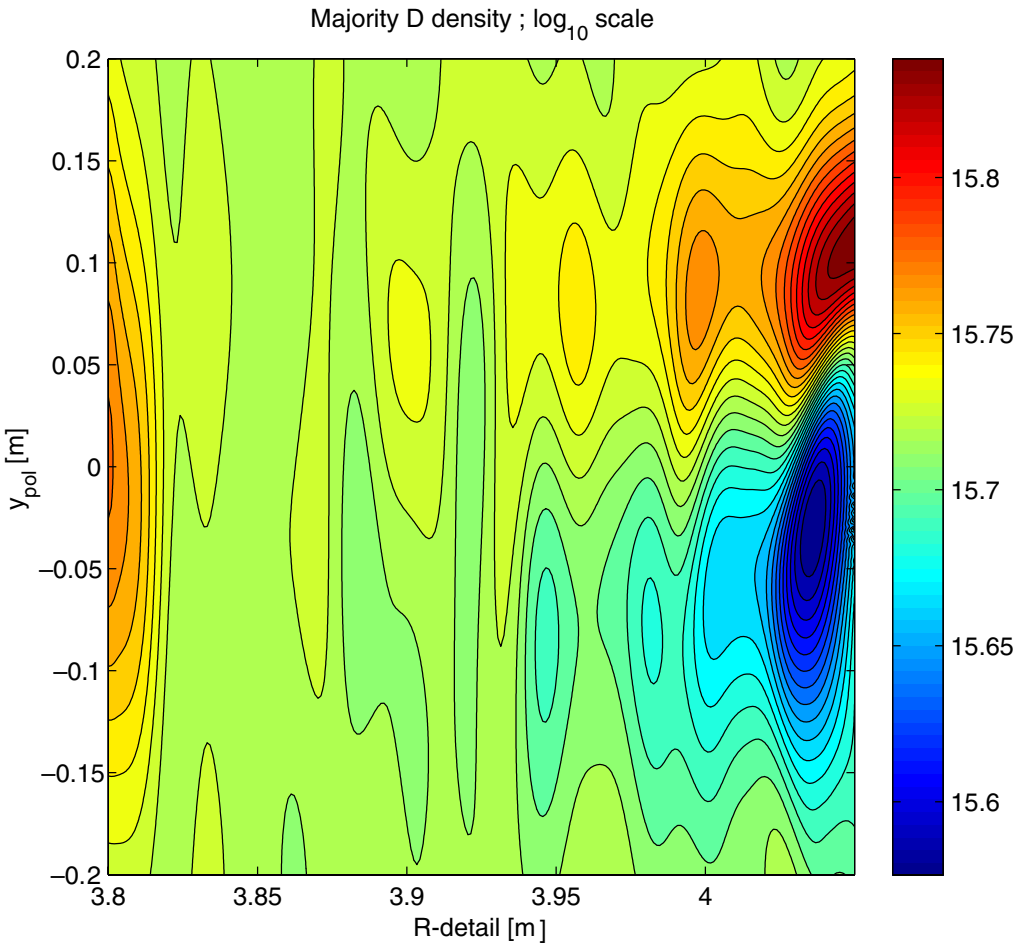

Figure 3. 10-log of the RF modified majority D density profile in front of the antenna.

scales as $|v_i| \approx Z_i|E|^2/[LA_iB_o\omega^2]$, where L is the scalelength on which the ponderomotive potential varies. Hence (see also the previous section), drift velocities reach values of the order of 1–10 m s^{-1} in typical present-day tokamak circumstances. Such velocities are similar in magnitude to the radial pinch velocities quoted in transport studies (see, e.g., [22, 23]) and to the drift due to the finite ∇B responsible for individual particle orbits deviating from magnetic field lines (see, e.g., [24]).

However, even in the relatively cold plasma edge, the thermal velocity is significantly larger than the ponderomotive drift. Whereas the rapid cyclotron oscillation disappears when averaging on the fast time scales so that the perpendicular component of the RF-induced drift is more relevant on average than the gyro-rotation term, the thermal parallel motion is much larger than the parallel RF-induced ponderomotive drift. Thermalization would yield an average $v_\parallel = 0$ when integrated over a population in thermodynamical equilibrium (hereby making the parallel drift component relevant as well), but it is more likely that the small connection lengths connecting solid objects along field lines leave not enough time for a population to thermalize. Far behind the last closed flux surface and inside the antenna box in particular, it is clear that a better description of the plasma–wave interplay is needed to get a better grip on the flow dynamics. The onset to a more rigorous description is discussed in this section.

An important RF-related $\vec{E} \times \vec{B}$ drift discussed in the antenna modeling literature (see, e.g., [3, 18]) and closely related to the velocity discussed in this paper involves an electric field $\vec{E} = -\nabla\Phi$ derived from a rectified potential Φ. The latter is related to the voltage difference $V_{\rm RF} = \int \mathrm{d}\vec{x}_\parallel.\vec{E}$—measured along a magnetic field line and in which $\vec{E}$ is the RF electric field—through $\Phi = C|V_{\rm RF}|$. Adopting a 1D parallel plate capacitor model and integrating the ensuing sheath equations of the thin plasma between the plates numerically, Riyopoulos [25] and Myra [26] found a value for the factor C linking the fast and slow wave dynamics; it typically takes values around 0.5. It is found that various parameters (e.g. density, orientation of the ion flow and that of the magnetic field) have a nonnegligible impact on the results, details being sensitive to what happens in the first few Debye lengths away from the capacitor plates, where charge neutrality is violated. In view of the sensitivity of the results, Riyopoulos notes in his conclusions that 'the development of a 2D sheath theory seems essential to further improve the description of magnetized sheaths' beyond the simplified model describing the sheath dynamics consistent with an *imposed* 1D voltage driven electric field $E = -\mathrm{d}V/\mathrm{d}x$ between two capacitor plates. As Riyopoulos and Myra address the sheath dynamics (and reveal its sensitivity) omitting the details of the wave physics brought about by the plasma, one may wonder if such

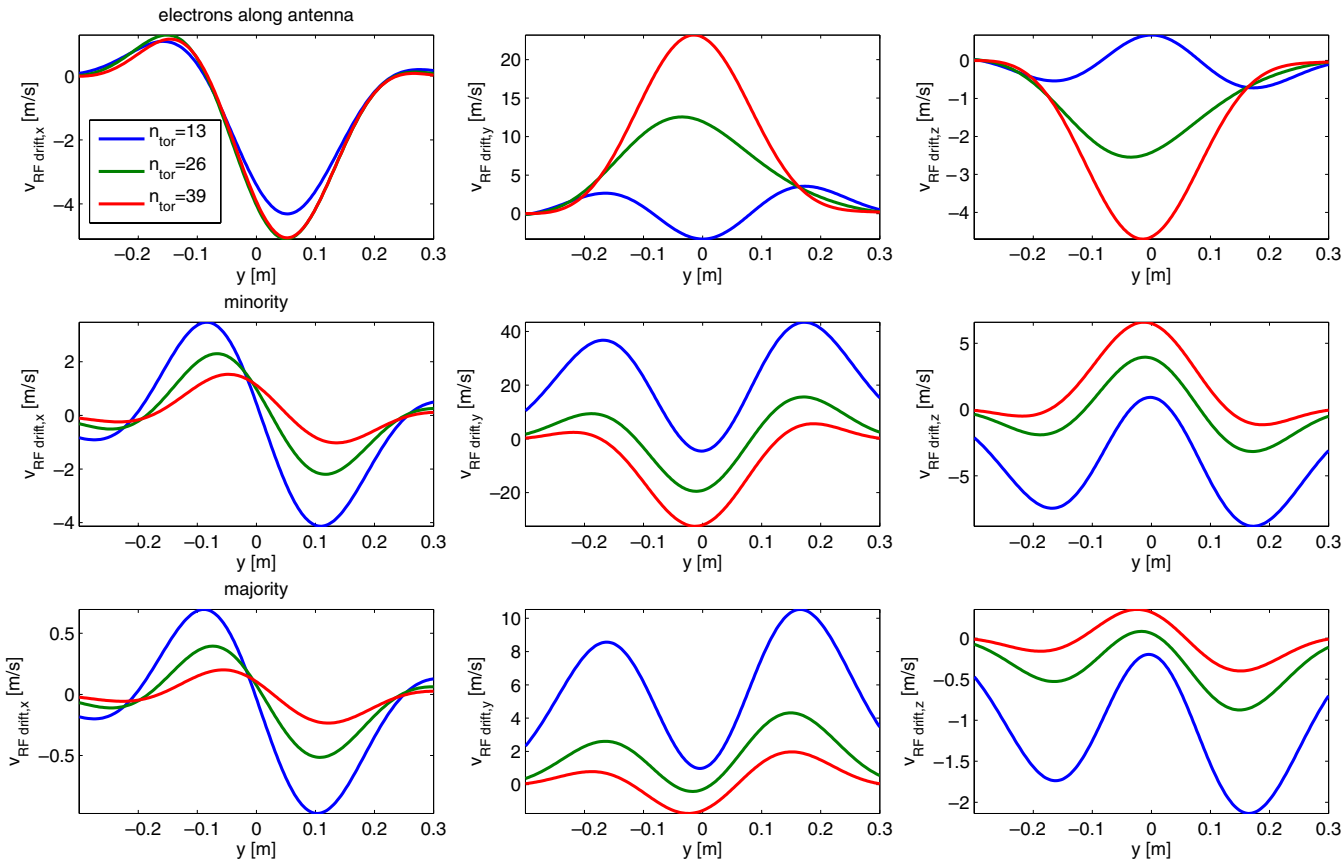

Figure 4. Drift velocity components along the antenna.

findings can indeed be applied to describe the dynamics in the *whole* antenna region—as opposed to the thin sheath region—in the presence of 3D electromagnetic fields that respond to and interact with the local density and magnetic field and are not just passively driven. In view of the richness of the subject, a discussion on the dynamics of the cold plasma fast and slow waves close to metallic objects is reserved to a separate study [16] while the focus in this paper is on the wave dynamics in the region *beyond* the sheath and on a scale length well beyond the first few Debye lengths close to metallic objects. Combining both descriptions will either justify the use of the relation $\Phi = C|V_{\rm RF}|$ beyond its 1D capacitor plate application, or will give hints on how it can be generalized. Either way, it seems essential to account for the slow time scale dynamics and their impact on what happens on the fast time scale (both in the sheath region where charge neutrality is strongly violated, and away from it) in a more rigorous way. An elegant solution that maximally builds on existing knowledge would be to generalize the sheath boundary condition as proposed by Myra and D'Ippolito [8–12] to account for the sheath physics and connect it to a 'nonsheath' model that accounts for the 3D evolution of both the slowly varying electrostatic $\vec{E}_o = -\nabla\Phi$ responsible for zero-order flows and the rapidly varying $\vec{E}_{(RF)}$ together with the relevant plasma parameters (density and flow velocity) away from the direct proximity of metallic objects. In spite of the importance of such a more global assessment, this is a vast topic well beyond the scope of this paper, which mainly lists a number of arguments to show that the standard modeling used to describe the antenna region is far from mature. A sketch of a plausible set of equations to better capture the plasma–wave cross-talk is discussed next.

The main conclusion from the previous section is that the usual cold plasma description allows one to predict that RF waves induce density modifications in front of the launcher, whereas arguments were just presented why a more sophisticated model is required to describe the processes more rigorously in particular to incorporate RF sheath effects, which occur on Debye scale length very close to metallic objects and have a better grip on the flows driven in the whole antenna region. Apart from the fact that the back-coupling of the net effect of the fast dynamics on the slow time scale was not rigorously accounted for here, the effect of transport has so far been omitted and the considered geometry was taken as simple as possible.

Including the physics of the impact of the waves on the tokamak plasma rigorously, i.e. accounting for the cross-talk between charged particles and electromagnetic waves in an environment subjected to the influence of a strong confining magnetic field, requires going well beyond the plasma models commonly adopted for describing wave-plasma interactions: the simplest possible description allowing one to model the dynamics self-consistenty requires going back to the first-principle equations combining Maxwell's equations with a two-fluid plasma model (one type of electrons and one type of ions) containing the equation of motion and the continuity equation, possibly augmented with an energy equation for each

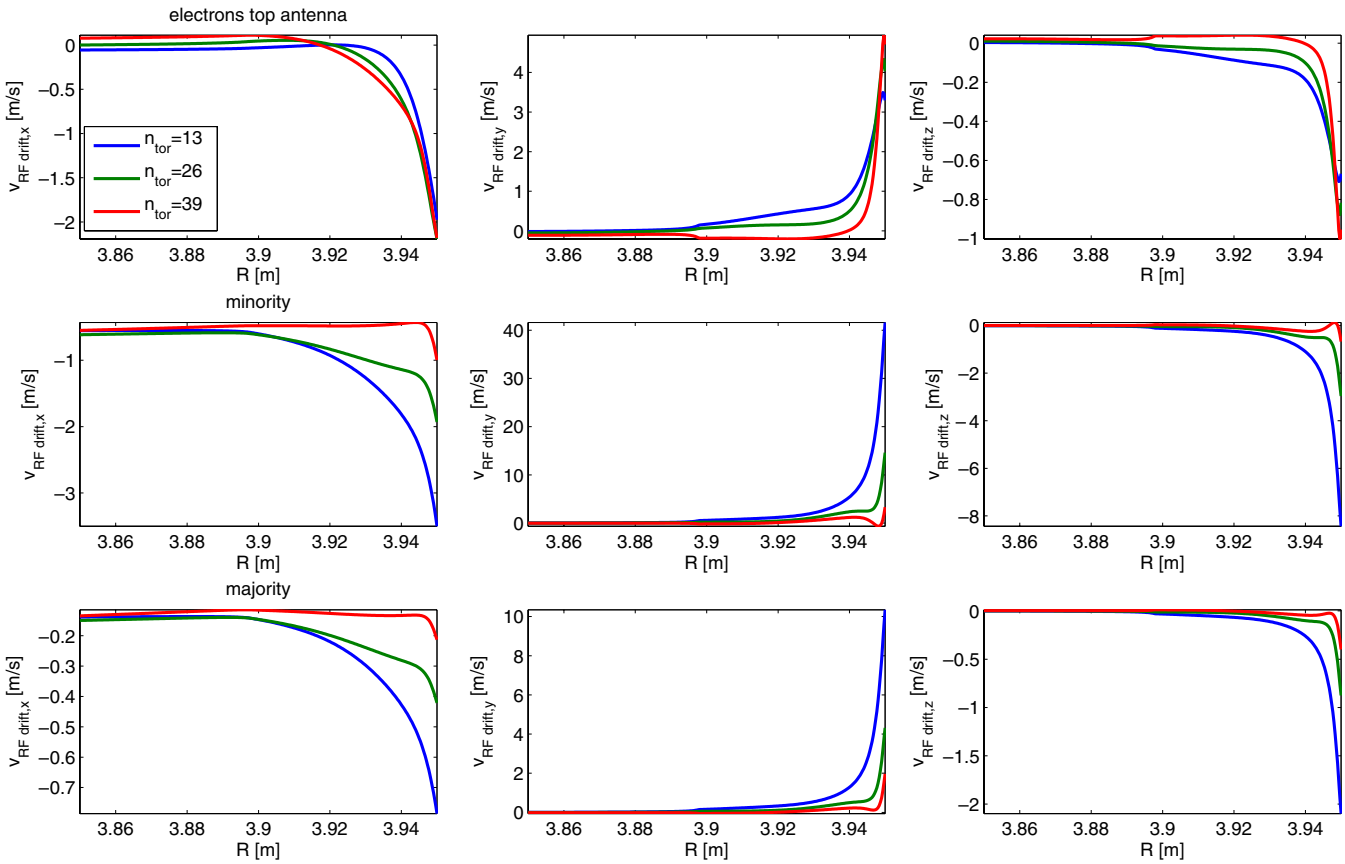

Figure 5. Drift velocity components at the top of the antenna.

type of particles if the wave absorption in the antenna region—and in particular in the RF sheath—is to be addressed in sufficient detail to make senseful predictions about RF induced sputtering, and to acquire a feeling of how the reduction in coupling caused by the RF induced density modification can be avoided. In principle, all needed equations and techniques are already available from basic literature (see, e.g., [14, 15] and references therein) but in practice the task represents a challenge that has—to date—never been addressed in the context of antenna near-field studies because of the huge disparity in length and time scales involved: antennas have lengths of the order of a meter, while the sheath is submillimetric; the RF time scale is in the MHz range while the drifts are in the Hz–kHz range. Since the fast time scale wave dynamics causes slow time scale modifications and modifications of the latter have an impact on the fast time scale phenomena, the resulting equations need to be solved accounting for the details on two very different time scales and should be solved iteratively to consistently account for the cross-talk between fast and slowly varying quantities.

A more rigorous description of the wave dynamics mainly incorporates a generalization of the usual cold plasma dielectric tensor in order to include the presence of zero-order drifts. The usual RF wave model is based on the simplified equation of motion

$$-\mathrm{i}\omega\vec{v}_1 = \frac{q}{m}[\vec{E} + \vec{v}_1 \times \vec{B}_o] = \frac{q}{m}\vec{E} + \Omega\vec{v}_1 \times \vec{e}_\parallel,$$

which allows one to relate the velocity to the electric field via an operator $\boldsymbol{M}$,

$$\boldsymbol{M}\vec{v}_1 = \begin{pmatrix} -\mathrm{i}\omega & -\Omega & 0 \\ +\Omega & -\mathrm{i}\omega & 0 \\ 0 & 0 & -\mathrm{i}\omega \end{pmatrix} . \begin{pmatrix} v_{1,\perp 1} \\ v_{1,\perp 2} \\ v_{1,//} \end{pmatrix},$$

acting on the perturbed velocity. This operator is readily inverted to allow writing down an expression for the current density and thus for the dielectric tensor. With drifts, it is generalized to

$$\boldsymbol{M}\vec{v}_1 = -\mathrm{i}\omega\vec{v}_1 + \vec{v}_o.\nabla\vec{v}_1 + \vec{v}_1.\nabla\vec{v}_o + \vec{v}_1.\nabla\vec{v}_1 - \frac{q}{m}\vec{v}_1 \times \vec{B}_o - \frac{q}{m}\vec{v}_1 \times \vec{B}_1,$$

which can no longer be inverted in the same way because of the nonlinear contributions that appear. Assuming the perturbation terms are rapidly varying but very small, adopting the quasilinear approach allows one to neglect these terms in the first order equation, while casting their—nonzero—average over the rapid oscillations into the zero order equation of motion. The $\boldsymbol{M}$ operator then reduces to

$$\boldsymbol{M}\vec{v}_1 = -\mathrm{i}\omega\vec{v}_1 + \vec{v}_o.\nabla\vec{v}_1 + \vec{v}_1.\nabla\vec{v}_o - \frac{q}{m}\vec{v}_1 \times \vec{B}_o.$$

If its inversion can be realized, this provides an explicit formula for the perturbed velocity and thus a generalization of the philosophy of the cold plasma dielectric tensor derivation. In a homogeneous plasma, this is immediate: Fourier analysis

allows one to write

$$M\vec{v}_1 = \begin{pmatrix} \mathrm{i}[\vec{v}_o.\vec{k} - \omega] + \frac{\partial v_{o,x}}{\partial x} & \frac{\partial v_{o,x}}{\partial y} - \Omega & \frac{\partial v_{o,x}}{\partial z} \\ \frac{\partial v_{o,y}}{\partial x} + \Omega & \mathrm{i}[\vec{v}_o.\vec{k} - \omega] + \frac{\partial v_{o,y}}{\partial y} & \frac{\partial v_{o,y}}{\partial z} \\ \frac{\partial v_{o,z}}{\partial x} & \frac{\partial v_{o,z}}{\partial y} & \mathrm{i}[\vec{v}_o.\vec{k} - \omega] + \frac{\partial v_{o,z}}{\partial z} \end{pmatrix} \cdot \begin{pmatrix} v_{1,x} \\ v_{1,y} \\ v_{1,z} \end{pmatrix},$$

which can be inverted analytically. In an inhomogeneous plasma this simple inversion can no longer be carried out. Although it still makes sense to perform a Fourier analysis in ignorable directions, the variation across the sheath layer that is formed close to a metallic object discourages using a Fourier analysis approach in that directions so it is more practical to directly solve the full system of equations in that case. The field pattern is described by Maxwell's equations, while for each of the considered species types the solutions of the equation of motion and the continuity equation are needed. One finds the set of equations

$$\begin{aligned} &N_{o,\alpha}\left[-\mathrm{i}\omega\vec{v}_{1,\alpha} + \vec{v}_{1,\alpha}.\nabla\vec{v}_{o,\alpha} + \vec{v}_{o,\alpha}.\nabla\vec{v}_{1,\alpha}\right] - N_{o,\alpha}\frac{q_\alpha}{m_\alpha}\vec{v}_{1,\alpha}\times\vec{B}_o \\ &+N_{1,\alpha}\left[\frac{\partial\vec{v}_o}{\partial t} + \vec{v}_o.\nabla\vec{v}_o\right] = -\frac{kT_\alpha}{m_\alpha}\nabla N_{1,\alpha} \\ &+N_{1,\alpha}\frac{q_\alpha}{m_\alpha}\left[\vec{E}_o + \vec{v}_{o,\alpha}\times\vec{B}_o\right] + N_{o,\alpha}\frac{q_\alpha}{m_\alpha}\left[\vec{E}_1 + \vec{v}_{o,\alpha}\times\vec{B}_1\right], \\ &\mathrm{i}\omega N_{1,\alpha} = \nabla.\left[N_{o,\alpha}\vec{v}_{1,\alpha} + N_{1,\alpha}\vec{v}_{o,\alpha}\right] \\ &\nabla\times\vec{E}_1 = \mathrm{i}\omega\vec{B}_1, \\ &\nabla\times\vec{B}_1 = -\frac{\mathrm{i}\omega}{c^2}\vec{E}_1 + \mu_o\sum_\alpha q_\alpha\left[N_{1,\alpha}\vec{v}_{o,\alpha} + N_{o,\alpha}\vec{v}_{1,\alpha}\right], \end{aligned}$$

which describe the dynamics on the fast time scale and driven at the frequency ω, while

$$\begin{aligned} &N_{o,\alpha}\frac{\partial}{\partial t}\vec{v}_{o,\alpha} = \langle\mathrm{i}\omega N_{1,\alpha}\vec{v}_{1,\alpha}\rangle - N_{o,\alpha}\vec{v}_{o,\alpha}.\nabla\vec{v}_{o,\alpha} - \frac{kT_\alpha}{m_\alpha}\nabla N_{o,\alpha} \\ &+N_{o,\alpha}\frac{q_\alpha}{m_\alpha}\left[\vec{E}_o + \vec{v}_{o,\alpha}\times\vec{B}_o\right] - N_{o,\alpha}\langle\vec{v}_{1,\alpha}.\nabla\vec{v}_{1,\alpha}\rangle \\ &-\langle N_{1,\alpha}\vec{v}_{1,\alpha}\rangle.\nabla\vec{v}_{o,\alpha} - \langle N_{1,\alpha}\vec{v}_{o,\alpha}.\nabla\vec{v}_{1,\alpha}\rangle + \frac{q_\alpha}{m_\alpha}\langle N_1\vec{E}_1\rangle \\ &+\frac{q_\alpha}{m_\alpha}N_{o,\alpha}\langle\vec{v}_{1,\alpha}\times\vec{B}_1\rangle + \frac{q_\alpha}{m_\alpha}\langle N_{1,\alpha}\vec{v}_{1,\alpha}\rangle\times\vec{B}_o \\ &+\frac{q_\alpha}{m_\alpha}\langle N_{1,\alpha}\vec{v}_{o,\alpha}\times\vec{B}_1\rangle \\ &\frac{\partial}{\partial t}N_{o,\alpha} = -\nabla.N_{o,\alpha}\vec{v}_{o,\alpha} - \langle\nabla.N_{1,\alpha}\vec{v}_{1,\alpha}\rangle, \\ &\frac{\partial}{\partial t}\vec{B}_o = -\nabla\times\vec{E}_o, \\ &\frac{1}{c^2}\frac{\partial}{\partial t}\vec{E}_o = \nabla\times\vec{B}_o - \mu_o\sum_\alpha q_\alpha\left[N_{o,\alpha}\vec{v}_{o,\alpha} + \langle N_{1,\alpha}\vec{v}_{1,\alpha}\rangle\right] \end{aligned}$$

describes the dynamics on the slow time scale. Here, $\langle\ldots\rangle$ denotes the time average over a full cycle of the driver, i.e., $\langle AB\rangle = \langle\mathrm{Re}[A]\mathrm{Re}[B]\rangle = 1/2\mathrm{Re}[A^*B]$ for complex perturbed quantities sharing the exponential factor $\exp[-\mathrm{i}\omega t]$.

Whereas the problem at hand involves analyzing a fairly straightforward second-order partial differential equation when omitting the back-coupling and limiting the description to the dominant wave type excited by the antenna, mastering the global problem involves solving two sets of 14 (when not including an energy aside from the momentum equation) or 16 (with an energy equation) coupled equations—one set for each of the time scales—and represents a major numerical challenge in view of the short wavelength of some of the wave types; by eliminating a maximum of dependent variables, it can be shown that there are now eight rather than four possible wave types in this simplest possible extension.

The above equations *do not* contain terms accounting for the gradients of quantities and thus terms of the type equation (1) should be added to the description to include the impact of the deviation of $\vec{x}$ from $\vec{x}_o$ during a driver cycle, unless other terms dominate them and allow them being neglected. Such a much more rigorous approach has - to the authors' knowledge—not yet been attempted to date and is the topic of a future work on modeling the antenna near-field.

As a concluding remark, it is worthwhile to mention that the advent of massive parallelization has allowed for an alternative type of approach to be explored for modeling high-frequency waves in tokamaks: finite difference time domain (FDTD) solvers can track the wave evolution on the cyclotron time scale and are thus able in a natural way to describe the net averaging effect brought about by the ponderomotive force when integrating the relevant equations over sufficiently long times *without* needing to separate 'fast' and 'slow' dynamics. Smithe pioneered this approach in the context of ICRH wave propagation in tokamaks [27] and, e.g., adopted it to address the wave launch as well as the sheath region problem [28, 29], be it in the capacitor plate limit mentioned earlier. Although it will require significant computer resources to cover both time scales for actual 3D problems, FDTD solvers potentially constitute an elegant and intuitive way to address the wave launch, sheath, density evolution and flow creation problems simultaneously.

7. Summary

In this brief paper it is shown that high-frequency waves give rise to net velocity drifts close to the antennas. Not only the parallel electric field is of importance; close to cyclotron layers—where the denominator of the (cold plasma) drift velocity goes through zero—the perpendicular components are responsible for the major flow caused by the ponderomotive effect discussed here. Poloidal field inhomogeneity (e.g. at the poloidal ends of the antenna) gives rise to radial excursion, while radial inhomogeneity yields a poloidal flow. As the

plasma supports both fast and slow waves, the wave dynamics is a sensitive function of the density faced by the antennas. The drift velocities and ensuing density change found here are qualitatively in agreement with experimentally observed scaling of the density with the antenna phasing but it mainly underlines the need for a more self-consistent description of the antenna near-field region. A sketch is given of a possible road ahead.

References

[1] Louche F *et al* 2011 *Nucl. Fusion* **51** 103002
[2] Lamalle P U *et al* 2003 *30th EPS Conf. on Controlled Fusion and Plasma Physics (St. Petersburg, 7–11 July)* vol 27A ECA P-1.193
[3] D'Ippolito D A *et al* 1998 *Nucl. Fusion* **38** 1543
[4] Messiaen A *et al* 2011 *Plasma Phys. Control. Fusion* **53** 085020
[5] Jacquet P *et al* 2012 *Nucl. Fusion* **52** 042002
[6] Lancellotti V *et al* 2006 *Nucl. Fusion* **46** S476
[7] Colas L *et al* 2007 *Plasma Phys. Control. Fusion* **49** B35
[8] Myra J R *et al* 1994 *Phys. Plasmas* **1** 2891
[9] D'Ippolito D A *et al* 2006 *Phys. Plasmas* **13** 102508
[10] D'Ippolito D A *et al* 2009 *Phys. Plasmas* **16** 022506
[11] D'Ippolito D A *et al* 2010 *Phys. Plasmas* **17** 072508
[12] D'Ippolito D A *et al* 2011 *J. Nucl. Mater.* **415** S1001
[13] Jacquot J *et al* 2012 *Proc. 39th EPS Conf. and 16th Int. Congress on Plasma Physics (Stockholm, 2–7 July)* paper P2.038
[14] Stix T H 1992 *Waves in Plasmas* (New York: Springer)
[15] Swanson D G 1989 *Plasma Waves* (New York: Academic)
[16] Van Eester D *et al* 2012 Connection coefficients for cold plasma wave propagation near metallic surfaces *Plasma Phys. Control. Fusion* submitted
[17] Fukuyama A *et al* 1982 *J. Phys. Soc. Japan* **51** 1010
[18] Becoulet M *et al* 2002 *Phys. Plasmas* **9** 2619
[19] Bobkov V *et al* 2010 *Nucl. Fusion* **50** 035004
[20] Kaye A *et al* 1994 *Fusion Eng. Des.* **74** 1
[21] Weynants R R 2009 *Proc. 18th Top. Conf. on RF Power in Pasmas (Ghent, 24–26 June)* **1187** 3
[22] Valisa M *et al* Radio-frequency power injection and impurity profile control in JET *Proc. 36th EPS Conf. on Plasma Physics (Sofia, 29 June–3 July)* also *Report EFDA JET* CP(09)06/10
[23] Valisa M *et al* 2011 Metal impurity transport control in JET H-mode plasmas *Nucl. Fusion* **51** 033002 also *Report* EFDA JET PR(10)36
[24] de Blank H 2012 *Proc. Carolus Magnus Summer School, Fusion Science and Technology (Weert, 4–16 September 2011)* **61** 61
[25] Riyopoulos S 1999 *Phys. Rev.* E **59** 1111
[26] Myra J R *et al* 1990 *Nucl. Fusion* **30** 845
[27] Smithe D 2007 *Phys. Plasmas* **14** 056104
[28] Smithe D 2007 *J. Phys.: Conf. Ser.* **78** 012069
[29] Smithe D *et al* 2008 *50th APS-DPP Conf. (Austin, TX, 2008)*